Robust Gradient-Based 3-D/2-D Registration of CT and MR to X-Ray Images

Primož Markelj*, Dejan Tomaževič, Franjo Pernuš, and Boštjan Likar

Abstract—One of the most important technical challenges in image-guided intervention is to obtain a precise transformation between the intrainterventional patient's anatomy and corresponding preinterventional 3-D image on which the intervention was planned. This goal can be achieved by acquiring intrainterventional 2-D images and matching them to the preinterventional 3-D image via 3-D/2-D image registration. A novel 3-D/2-D registration method is proposed in this paper. The method is based on robustly matching 3-D preinterventional image gradients and coarsely reconstructed 3-D gradients from the intrainterventional 2-D images. To improve the robustness of finding the correspondences between the two sets of gradients, hypothetical correspondences are searched for along normals to anatomical structures in 3-D images, while the final correspondences are established in an iterative process, combining the robust random sample consensus algorithm (RANSAC) and a special gradient matching criterion function. The proposed method was evaluated using the publicly available standardized evaluation methodology for 3-D/2-D registration, consisting of 3-D rotational X-ray, computed tomography, magnetic resonance (MR), and 2-D X-ray images of two spine segments, and standardized evaluation criteria. In this way, the proposed method could be objectively compared to the intensity, gradient, and reconstruction-based registration methods. The obtained results indicate that the proposed method performs favorably both in terms of registration accuracy and robustness. The method is especially superior when just a few X-ray images and when MR preinterventional images are used for registration, which are important advantages for many clinical applications.

Index Terms—Image-guided, intensity gradients, intervention, surgery, three-dimensional/two-dimensional (3-D/2-D) registration.

I. INTRODUCTION

MEDICAL imaging has long been crucial in providing the clinician with information about the internal anatomy of the human body, facilitating medical diagnosis, monitoring of disease or treatment progress, and planning of medical interventions. A successful intervention commonly requires that the clinician, using knowledge accumulated over years of training, in his mind establishes the correspondence between the patient

and the information in his preoperative images. The desire to facilitate the establishment of correspondence and the constant need to make the interventions even more accurate and less invasive gave rise to the discipline of image-guided intervention (IGI). The essence of IGI is to help to diagnose, plan, simulate, guide, or otherwise assist an interventionalist or possibly a robot in performing an interventional procedure (surgery, radiation therapy, chemotherapy, biopsy, etc.) by using high-quality preinterventional medical data, usually computed tomography (CT) or magnetic resonance (MR) images in the intervention room. One of the most important technical challenges of an IGI system is to obtain a precise transformation between the patient's anatomy in the interventional coordinate system and any 3-D point in the preinterventional image coordinate system. This can be achieved by registering the preinterventional data either directly to the patient or indirectly to one or more 3-D or 2-D images of the patient acquired during intervention. The correct transformation allows precise 3-D positioning of the interventional instruments in preinterventional images relative to the final target and nearby vulnerable structures that are to be avoided during the intervention. IGI is therefore most beneficial for surgical applications (neurosurgery [1], [2], spinal surgery [3], orthopedics [4]–[6]) and radiotherapy [7]–[10], where the target must be effectively treated (radiated) while minimizing damage to the healthy tissue.

With the widespread use of numerous 3-D and 2-D imaging modalities, registration of images of different modalities and dimensions has become an important issue of IGI. Commonly, X-ray or ultrasound imaging is used to acquire images during intervention, while CT and/or MR images are typically the preinterventional modalities of choice, yielding detailed 3-D anatomical information that can be efficiently exploited if registered to the intrainterventional images. A vast number of 3-D/2-D registration methods proposed in the past can be classified according to many criteria, such as the nature of registration basis, the nature and domain of transformation, optimization procedure, modalities involved, etc., [11]. Most traditionally the 3-D/2-D methods can be coarsely classified into feature-based and intensity-based methods. However, to further discriminate and survey the major characteristics of the existing methods, we classify the methods into four categories, namely into the feature-based, intensity-based, gradient-based, and reconstruction-based methods.

Feature-based 3-D/2-D registration methods [4], [12]–[17] are concerned with finding the transformation that minimizes the distances between corresponding features extracted from the preinterventional image or anatomical model and the intrainterventional image. The features can be either extrinsic, requiring attachment of fiducial markers, or intrinsic, obtained

by extracting features of anatomical structures. The fiducial markers are either implanted into bone of the patient or skin-affixed. Because implanted fiducials yield very accurate registrations, they are commonly used to define the reference or "gold" standard registration [18], [19]. However, such implantation is invasive and may be inconvenient to the patient. On the other hand, due to skin elasticity, fiducials attached to skin produce less accurate registration results. The less invasive but more sophisticated intrinsic approach uses points, contours, or surfaces extracted from image data sets [4], [13]–[15] or from statistical models of anatomy [16], [17]. Some form of outlier removal is commonly used to refine the features used for registration. Extraction of geometrical features greatly reduces the amount of data, which in turn makes the registration fast. However, the accuracy of the procedure is directly dependent upon the accuracy of the segmentation, which by itself is a nontrivial procedure to perform automatically, while manual segmentation is time consuming and subjective.

Intensity-based registration methods use all the image data available by matching image intensities [2], [3], [7]–[9], [20]–[23]. To compare intensities of 3-D CT and 2-D X-ray images in the 2-D domain, projection images called digitally reconstructed radiographs (DRRs) are created from the CT image. The matching process is carried out by optimizing the measure of similarity between the DRR(s) and the X-ray image(s). A variety of similarity measures was proposed in the past [2], [3], [21], [22], among which the optimal similarity measure seems to be application specific, although gradient and correlation based similarity measures yield the most accurate results [8], [21], [23], [24]. By using all the available information, the intensity-based methods generally outperform the intrinsic feature-based methods in terms of accuracy but the large amount of data makes intensity-based methods rather slow. This drawback can be reduced by using faster methods for DRR generation [25]–[27] or by reducing the matching to a region of interest [2], [3], [7], [8], [21]–[23], all of which can be further accelerated using hardware-acceleration methods [8]. However, by projecting a high-quality 3-D image into 2-D, valuable 3-D information may be lost. Furthermore, since there is practically no correspondence between MR-based DRRs and X-ray images, the intensity-based methods are generally not suitable for registration of MR to X-ray images.

In gradient-based registration methods a subset of 3-D intensity gradients is compared to X-ray gradients [28] or a subset of 2-D X-ray gradients is compared to 3-D intensity gradients [6]. Gradient-based methods are accurate and the reduced set of significant gradients makes the gradient-based methods fast. Furthermore, as 3-D gradients can also be extracted from MR images, MR to X-ray 3-D/2-D registration is also possible [28]. However, registration of intensity gradients typically results in poor registration convergence, if the initial misregistration is large [6], [28].

Most recently, reconstruction-based methods have been proposed, that first reconstruct a 3-D image from a few fluoroscopic or X-ray images [29], [30], and then perform 3-D/3-D registration. To overcome the problem of poor quality of a 3-D image reconstructed from only a few fluoroscopic X-ray images, a robust mutual information based similarity measure, called asymmetric multifeature mutual information, has recently been proposed [29], [31]. The measure uses additional spatial features in the form of intensity gradients. An extensive evaluation has shown that the 3-D/2-D reconstruction-based method [29] outperforms the gradient-based method [28] in terms of capture range and success rate. However, reconstruction-based methods are slower and typically require more intrainterventional images, especially for MR to X-ray registration, which may be a limitation for clinical use.

The aim of this work is to combine the advantages of gradient-based and reconstruction-based methods so as to obtain a robust 3-D/2-D registration method for both 3-D CT and MR preinterventional images that will require only a small number of 2-D intrainterventional images. The proposed method is based on matching 3-D gradients of 3-D images to 3-D gradients coarsely reconstructed from 2-D images. To improve the process of finding the correspondences between the two sets of gradients and thereby the robustness of the registration method, hypothetical correspondences are searched for along normals to anatomical structures in 3-D images, while the final correspondences are established in an iterative process, combining the robust random sample consensus algorithm (RANSAC) [32] and special gradient matching criterion function. The novel method has been evaluated using the standardized evaluation methodology for 3-D/2-D registration [33], which enables objective comparison to some of the well-known registration methods [21], [28], [29].

II. METHOD

The goal of rigid 3-D/2-D registration is to find a transformation $\mathbf{T}$ that relates the coordinate system $\mathbf{S}_{\text{pre}}$ of the 3-D preinterventional image to the world or patient coordinate system $\mathbf{S}_w$ (Fig. 1). To estimate this transformation by using 2-D intrainterventional images, the X-ray acquisition system needs to be calibrated so that the transformation $\mathbf{T}_c$ between the intrainterventional image coordinate system $\mathbf{S}_{\text{intra}}$ and the world coordinate system $\mathbf{S}_w$ is established [34]. We focus on the calculation of the six parameters $\mathbf{q} = (t_x, t_y, t_z, \omega_x, \omega_y, \omega_z)$ that define the rigid transformation $\mathbf{T}$ and relate the coordinate system $\mathbf{S}_{\text{pre}}$ of the preinterventional image to the world coordinate system $\mathbf{S}_w$. The description of the proposed method is divided into three subsections. The first describes the calculation of gradient fields, the second addresses the gradient correspondence maximization, while the third outlines the gradient-reconstruction based registration.

A. Calculation of Gradient Fields

The proposed method is based on the assumption that strong intensity gradients in 2-D X-ray images correspond to distinctive boundaries of anatomical structures in 3-D CT or MR images [28]. Using this idea, the 3-D preinterventional image is preprocessed to extract a set of strong intensity gradients $\mathbf{u}(\mathbf{p}_i)$; $i = 1, 2, \ldots, I$, that generally represent the surfaces and boundaries of anatomical structures and estimate the corresponding surface normals at 3-D points $\mathbf{p}_i$ defined in the coordinate system $\mathbf{S}_{\text{pre}}$ of the preinterventional image.
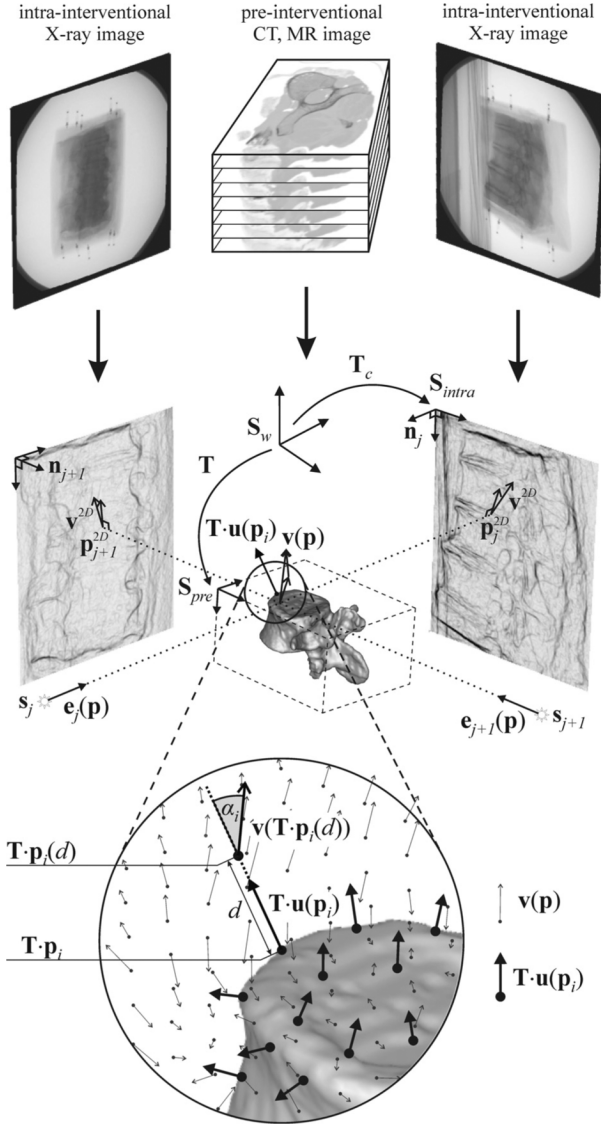
Fig. 1. 3-D/2-D registration procedure and corresponding geometrical setup for the registration of gradients $\mathbf{u}(\mathbf{p}_i)$ representing the boundaries of anatomical structures in a 3-D image and the coarsely reconstructed gradient field $\mathbf{v}(\mathbf{p})$ from the 2-D gradient images $\mathbf{v}^{2D}$.

To coarsely reconstruct the gradients from 2-D intrainterventional images, each 2-D intrainterventional image $j; j = 1, 2, \ldots, J$, is preprocessed to obtain its 2-D gradient field $\mathbf{v}^{2D}(\mathbf{p}_j^{2D})$. The extracted gradients $\mathbf{v}^{2D}(\mathbf{p}_j^{2D})$ from all J X-ray images are then back-projected into 3-D [28] and their information integrated in 3-D by simple summation so as to obtain a coarsely reconstructed 3-D gradient field $\mathbf{v}(\mathbf{p})$:

$$\mathbf{v}(\mathbf{p}) = \sum_{j=1}^{J} \frac{(\mathbf{n}_j \times \mathbf{v}^{2D}(\mathbf{p}_j^{2D})) \times \mathbf{e}_j(\mathbf{p})}{\mathbf{n}_j \cdot \mathbf{e}_j(\mathbf{p})} \cdot \frac{|\mathbf{p}_j^{2D} - \mathbf{s}_j|}{|\mathbf{p} - \mathbf{s}_j|} \quad (1)$$

where $\mathbf{p}$ is a 3-D position, $\mathbf{s}_j$ the position of the X-ray source of the jth 2-D image and $\mathbf{p}_j^{2D}$ the corresponding projection of $\mathbf{p}$ to the jth 2-D image, $\mathbf{n}_j$ the unit normal to the jth 2-D image, $\mathbf{e}_j(\mathbf{p})$ a unit vector defining the projection of point $\mathbf{p}$ to the jth 2-D image, and $\mathbf{v}^{2D}$ the extracted gradient in the jth 2-D image,

all defined in the world coordinate system $\mathbf{S}_w$ (Fig. 1). The first term in (1) represents the component of the gradient $\mathbf{v}^{2D}(\mathbf{p}_j^{2D})$ that is perpendicular to the projection beam $\mathbf{e}_j(\mathbf{p})$, while the second term represents the back-projection and corresponding scaling, which depends on the 3-D position of $\mathbf{p}$ [28].

In this way, the 3-D/2-D registration problem is translated to the problem of 3-D/3-D registration of a set of gradients $\mathbf{u}(\mathbf{p}_i)$ obtained from the 3-D preinterventional image and the coarsely reconstructed gradient field $\mathbf{v}(\mathbf{p})$ from the 2-D intrainterventional images.

B. Gradient Correspondence Maximization

Registration of the gradient sets $\mathbf{u}(\mathbf{p}_i)$ to $\mathbf{v}(\mathbf{p})$ is achieved by applying a transformation $\mathbf{T}$ to gradients $\mathbf{u}(\mathbf{p}_i)$ and maximizing the correspondences with the gradient field $\mathbf{v}(\mathbf{p})$, using a robust gradient-matching criterion function (CF), like the one proposed in [28]

$$\mathrm{CF}(\mathbf{T}, \mathbf{u}(\mathbf{p}_i), \mathbf{v}(\mathbf{p}))$$
$$= \frac{\sum_{i=1}^{I} |\mathbf{T} \cdot \mathbf{u}(\mathbf{p}_i)| \cdot |\mathbf{v}(\mathbf{T} \cdot \mathbf{p}_i)| \cdot f(\alpha_i)}{\sum_{i=1}^{I} |\mathbf{T} \cdot \mathbf{u}(\mathbf{p}_i)| \cdot \sum_{i=1}^{I} |\mathbf{v}(\mathbf{T} \cdot \mathbf{p}_i)|}, \quad (2)$$

where $\mathbf{T} \cdot \mathbf{u}(\mathbf{p}_i)$ denotes rigid transformation $\mathbf{T}$ of the gradients $\mathbf{u}(\mathbf{p}_i)$, i.e., rigid transformation $\mathbf{T} \cdot \mathbf{p}_i$ of the points $\mathbf{p}_i$ and corresponding rotations of gradients $\mathbf{u}(\mathbf{p}_i)$, and where $\mathbf{v}(\mathbf{T} \cdot \mathbf{p}_i)$ denotes the reconstructed gradients that correspond to the transformed gradients $\mathbf{T} \cdot \mathbf{u}(\mathbf{p}_i)$ at positions $\mathbf{T} \cdot \mathbf{p}_i$. The angle weighting function $f(\alpha_i)$ penalizes the angle difference α_i between the corresponding gradients $\mathbf{T} \cdot \mathbf{u}(\mathbf{p}_i)$ and $\mathbf{v}(\mathbf{T} \cdot \mathbf{p}_i)$

$$f(\alpha_i)$$
$$= \begin{cases} \cos^n(\alpha_i - m \cdot 180°), & |\alpha_i - m \cdot 180°| < 90° \\ 0, & \text{otherwise} \end{cases}.$$
$$(3)$$

The parameter n determines the sensitivity to angle difference α_i and the parameter $m; m = 0$ or 1, depends on the gradient directional correspondence between the imaging modalities. For example, $m = 0$ for CT or 3DRX to X-ray registration in which the corresponding registered intensity gradients are supposed to have the same directions, while $m = 1$ for MR to X-ray registration in which the corresponding registered intensity gradients have the opposite directions.

C. Gradient Reconstruction-Based Registration

Optimizing the CF in (2) yields a gradient reconstruction-based (GRB) registration method, which is similar to the gradient-based (GB) method [28], but with the criterion function with the coarsely reconstructed 3-D gradients from all the 2-D images and not by summing the criterion functions of individual 2-D images as in [28]. Similarly to GB, the GRB method should be fast, robust to outliers, and potentially accurate. However, because directly relating image gradients usually results in poor registration convergence, the GRB method should be useful for fine registration of coarsely preregistered images. To increase the convergence, the method is further sophisticated into the so-called robust gradient reconstruction-based (RGRB) method. The RGRB method combines the similarity measure
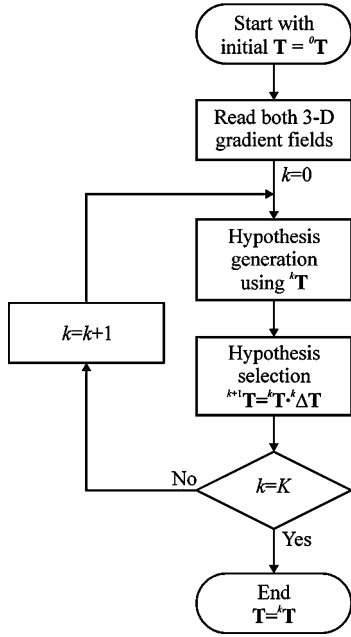
Fig. 2. Flowchart of the RGRB 3-D/2-D registration method.

(2) of the GRB method and a robust iterative registration scheme, interleaving the generation and selection of hypothetical gradient correspondences. In the hypothesis generation step, hypothetical point-to-point geometrical correspondences between each gradient $\mathbf{u}(\mathbf{p}_i)$ and the corresponding gradient field $\mathbf{v}(\mathbf{p})$ is established along a line defined by gradient $\mathbf{u}(\mathbf{p}_i)$. In the hypothesis selection step, the three point-to-point correspondences, defining the 3-D rigid transformation $\mathbf{T}$, that maximize the similarity (2) between all gradients $\mathbf{T} \cdot \mathbf{u}(\mathbf{p}_i)$ and the coarsely reconstructed gradient field $\mathbf{v}(\mathbf{p})$ are robustly selected among all pregenerated hypothetical point-to-point correspondences. The flowchart of the RGRB method is shown in Fig. 2.

First, in the hypothesis generation step of the kth iteration; $k = 1, 2, \ldots, K$, for the current registration transformation $^k\mathbf{T}$, hypothetical point-to-point geometrical correspondences $(\mathbf{p}_i, \mathbf{p}_i(d))$ between each gradient $\mathbf{u}(\mathbf{p}_i)$ and the coarsely reconstructed gradient field $\mathbf{v}(\mathbf{p})$ are established by finding the points $\mathbf{p}_i(d)$

$$\mathbf{p}_i(d) = \mathbf{p}_i + \mathbf{u}_e(\mathbf{p}_i) \cdot d \qquad (4)$$

at a distance d along the direction $\mathbf{u}_e(\mathbf{p}_i)$ of the gradient $\mathbf{u}(\mathbf{p}_i); \mathbf{u}_e(\mathbf{p}_i) = \mathbf{u}(\mathbf{p}_i)/|\mathbf{u}(\mathbf{p}_i)|$, using fixed sized increments [35]. The optimal point $\mathbf{p}_i(d^*)$ maximizes the point-to-point gradient similarity between the gradient $^k\mathbf{T} \cdot \mathbf{u}(\mathbf{p}_i)$ and corresponding gradient $\mathbf{v}(^k\mathbf{T} \cdot \mathbf{p}_i(d))$

$$\mathbf{p}_i(d^*) = \arg\max_{\mathbf{p}_i(d)} (|^k\mathbf{T} \cdot \mathbf{u}(\mathbf{p}_i)| \cdot |\mathbf{v}(^k\mathbf{T}$$
$$\cdot \mathbf{p}_i(d))| \cdot f(\alpha_i) \cdot {}^k g(d)) \quad (5)$$

where $^k g(d)$ is a monotonously decreasing weighting function that penalizes larger distances d from $\mathbf{p}_i$. The gradient $\mathbf{v}(^k\mathbf{T} \cdot \mathbf{p}_i(d))$ is obtained by interpolation of the gradient field $\mathbf{v}(\mathbf{p})$.

For a current registration transformation $^k\mathbf{T}$ and for each gradient $^k\mathbf{T} \cdot \mathbf{u}(\mathbf{p}_i)$, the obtained hypothetical point-to-point geometrical correspondence $(\mathbf{p}_i, \mathbf{p}_i(d^*)), i = 1, 2, \ldots, I$, thus represents the strongest and most colinear reconstructed gradient $\mathbf{v}(^k\mathbf{T} \cdot \mathbf{p}_i(d^*))$ along the line defined by $\mathbf{u}(\mathbf{p}_i)$.

Second, in the hypothesis selection step, the current registration transformation $^k\mathbf{T}$ is refined:

$$^{k+1}\mathbf{T} = {}^k\mathbf{T} \cdot {}^k\Delta\mathbf{T} \qquad (6)$$

by an incremental transformation $^k\Delta\mathbf{T}$ defined by the preselected hypothetical point-to-point geometrical correspondences $(\mathbf{p}_i, \mathbf{p}_i(d^*))$. This is carried out in a robust manner by adapting a random sample consensus algorithm (RANSAC) [32]. First, three, a minimal number for 3-D rigid transformation, point-to-point correspondences $(\mathbf{p}_i, \mathbf{p}_i(d^*))$ are repeatedly randomly selected L times; $l = 1, 2, \ldots, L$, from all I hypothetical correspondences, least-squares fitted to obtain the hypothetical incremental transformation $^{k,l}\Delta\mathbf{T}$ and hypothetical transformation $^{k+1,l}\mathbf{T} = {}^k\mathbf{T} \cdot {}^{k,l}\Delta\mathbf{T}$. Next, all gradients $\mathbf{u}(\mathbf{p}_i)$ are transformed by $^{k+1,l}\mathbf{T}$, yielding $^{k+1,l}\mathbf{T} \cdot \mathbf{u}(\mathbf{p}_i)$. Finally, the transformation that maximizes the sample consensus, i.e., the robust gradient-matching function (2) between all transformed gradients $^{k+1,l}\mathbf{T} \cdot \mathbf{u}(\mathbf{p}_i)$ and the coarsely reconstructed gradient field $\mathbf{v}(\mathbf{p})$, is selected

$$^{k+1}\mathbf{T} = \arg\max_{^{k+1,l}\mathbf{T}} \text{CF}(^{k+1,l}\mathbf{T}, \mathbf{u}(\mathbf{p}_i), \mathbf{v}(\mathbf{p})). \qquad (7)$$

The registration transformation $^k\mathbf{T}$ is iteratively; $k = 1, 2, \ldots, K$, refined by interleaving the hypothesis generation and the hypothesis selection step and changing (annealing) the distance weighting function $^k g(d)$ in (5) by the square root of the iteration index k

$$^k g(d) = g(d \cdot \sqrt{k}). \qquad (8)$$

Considering the Gaussian weighted function $g(d)$ and (8), results in the distance weighting function:

$$^k g(d) = e^{-\frac{1}{2} \cdot (\frac{d}{\sigma_d/\sqrt{k}})^2} \qquad (9)$$

where σ_d is the distance weighting parameter, defining the point-to-point correspondence-finding capture range $p_{\text{CR}}; p_{\text{CR}} = \sigma_d/\sqrt{k}$, that decreases by the square root of the iteration index k. Large initial $p_{\text{CR}}(k = 1, 2, 3, \ldots)$ enables the selection of hypothetical point-to-point correspondences at larger distances d and thereby increases the registration capture range. On the other hand, a smaller p_{CR} in the final iterations $(k \to K)$ generates more hypothetical point-to-point correspondences at smaller distances and thereby increases the registration accuracy.

Since the RGB method should be fast and accurate, while the RGRB method was designed to increase the robustness of the registration, we also introduce an extension of the RGRB by the GRB method, yielding the so-called RGRB extended method (RGRBe) as it might prove the most optimal solution in terms of speed, accuracy and robustness of registration. For implementation details the reader is referred to Section III-C.
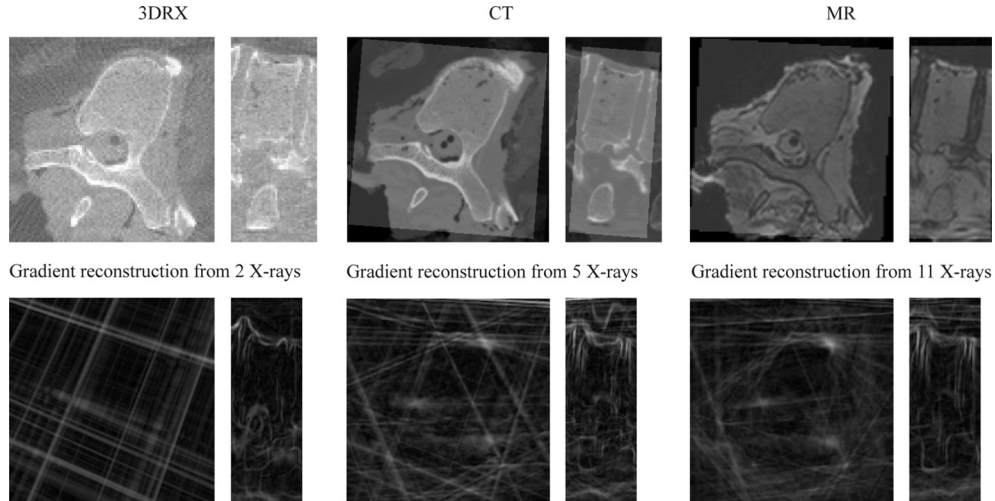
Fig. 3. Axial and lateral cross-sections taken from 3DRX, CT, and MR VOIs (top row from left to right), and coarsely reconstructed 3-D gradients from 2, 5, and 11 X-ray images (bottom row from left to right).

III. REGISTRATION EVALUATION

Evaluating the performance of a 3-D/2-D registration method requires a reference data set with known reference registration [36] also refered to as "gold" standard registration [19], [33]. A variety of validation approaches were used in the past, but to the best of our knowledge, currently there are only two reference data sets for 3-D/2-D registration publicly available [19], [33]. The publicly available[1] standardized evaluation methodology [33], consists of image data sets, reference transformations, regions of interest with corresponding centers of rotations, and measures for registration error, capture range, and success rate. Using this methodology in the current study, we were able to objectively compare the proposed method to three well-known 3-D/2-D registration methods. Namely, the intensity-based method (IB) [21] that compares 2-D digitally reconstructed radiographs (DRRs) and X-ray images using the gradient difference criterion function, the gradient-based method (GB) [28] that matches 3-D normals to bony surfaces and 2-D X-ray gradients back-projected into 3-D, and the reconstruction-based method (RB) [29] that integrates 2-D X-ray image information in 3-D and then performs 3-D/3-D image registration by a special multifeature mutual information similarity measure.

A. Experimental Data

The experimental image data consisted of 2-D X-ray images, CT and MR images, and 3DRX images of two defrosted segments of a spinal column with some soft tissue around both segments. One spinal segment consisted of three thoracolumbal vertebral bodies while the other of five thoracic vertebral bodies. The X-ray images were obtained by a clinical 3DRX system (Integris BV5000, Philips Medical Systems). A set of 100 X-ray images was acquired for each spinal segment in 8 s runs of 180° rotation around the imaged object. The images of the first and the second segment were acquired with image intensifier size of 380 and 310 mm, respectively. The 3DRX images were reconstructed from 100 X-ray projection images. The CT images were acquired with a clinical multislice CT scanner (MX8000,

[1]http://www.isi.uu.nl/Research/Databases/GS/

TABLE I
SIZES AND RESOLUTIONS OF THE X-RAY, 3DRX, CT, AND MR IMAGES

Modality	Segment	Resolution	Size
X-ray	1	0.63x0.63 mm^2	512^2
	2	0.53x0.53 mm^2	512^2
3DRX	1	0.87x0.87x0.87 mm^3	256^3
	2	0.52x0.52x0.52 mm^3	256^3
CT	1	0.31x0.49x0.31 mm^3	320x260x320
	2	0.31x0.49x0.31 mm^3	280x300x300
MR	1	1.00x0.75x0.75 mm^3	100x256x256
	2	1.00x0.88x0.88 mm^3	120x256x256

IDT 16, Philips Medical Systems). The MR images were obtained with a 1.5-T MR scanner (Gyroscan NT, Philips Medical Systems) using a sagittal 3-D turbo spin echo acquisition (turbo factor 29, $\mathrm{TR} = 1500$ ms, $\mathrm{TE} = 90$ ms). Examples of the acquired 3DRX, CT, and MR images are shown in Fig. 3 (top row), while the sizes and resolutions of all image data are given in Table I.

The reference registration between 3DRX images and 2-D projection images was already established in the process of creating 3DRX images, while the reference registrations of CT and MR images to 2-D X-ray images were obtained by a 3-D/3-D rigid registration of CT and MR images to the corresponding 3DRX images using the mutual information based registration method [37]. The error of the reference registration was evaluated to be similar to the error of 3-D/3-D registration, which was considered to be subvoxel and therefore at least as accurate as marker-based registration [38].

B. Evaluation Methodology

The mean target registration error (mTRE) was used to measure the distance of a vertebra from the reference position before and after registration. For the calculation of mTRE, positions of all voxels in a volume of interest (VOI), containing a whole vertebra, were used as target points [33]

$$\mathrm{mTRE} = \frac{1}{M} \sum_{m=1}^{M} \|\mathbf{T}_{\mathrm{reg}}\mathbf{p}_m - \mathbf{T}_{\mathrm{ref}}\mathbf{p}_m\| \tag{10}$$

where M is the number of target points $\mathbf{p}_m$, $\mathbf{T}_{\text{reg}}$ the registration determined by the registration algorithm and $\mathbf{T}_{\text{ref}}$ the reference or "gold" standard registration. To assess the accuracy, success rate, and capture range, registrations from 200 starting positions defined by randomly generated translations and rotations were performed for each VOI. The translations and rotations were chosen to yield mTRE values of the starting positions uniformly distributed in an interval from 0 to 20 mm, with 10 starting positions in each of the 1-mm-wide subintervals, as prepared by van de Kraats *et al.* [33]. Each registration was classified as successful if the mTRE after registration was smaller than a prespecified threshold of 2 mm. The success rate was defined as the number of successful registrations against the number of all registrations. The registration accuracy was computed as the average mTRE value of all successful registrations, while the capture range was defined as the distance from the reference position to the first 1-mm subinterval for which the registration was successful in less than 95% of all cases [33].

C. Implementation Details

The 3-D images were preprocessed using the 3-D Gaussian filter with the standard deviation of 0.3 mm for the CT and MR images, and of 0.5 mm for the 3DRX images. Next, the images were isotropically resampled to the resolution of 1 mm and subjected to the 3-D Canny edge detector. Finally, the resulting gradient images were thresholded as in [29] and [33] so as to extract the boundaries of anatomical structures and the corresponding set of gradients $\mathbf{u}(\mathbf{p}_i)$. Before preprocessing and gradient extraction, the MR images were corrected for intensity inhomogeneity by the information minimization method [39]. Spurious strong gradients corresponding to the spine phantom-to-background transition, which are not present in real MR spine images, were suppressed by simple morphological operations.

The X-ray images were blurred by the Gaussian filter with the standard deviation of 0.5 mm and subjected to the Roberts edge detector so as to calculate the intensity gradients $\mathbf{v}^{2D}(\mathbf{p}_j^{2D})$. The 3-D gradient fields $\mathbf{v}(\mathbf{p})$ were coarsely reconstructed in volumes of $137 \times 150 \times 145$ and $140 \times 200 \times 134$ image elements for the first and second spinal segment, respectively, with the isotropic resolution of 0.63 mm. To calculate the gradient-matching criterion function (2), the gradient $\mathbf{v}(\mathbf{T} \cdot \mathbf{p}_i)$ corresponding to each gradient $\mathbf{T} \cdot \mathbf{u}(\mathbf{p}_i)$ was determined using trilinear interpolation of the gradient field $\mathbf{v}(\mathbf{p})$. The value of the parameter n in the angle weighting function (3) was set to 4 as in [28].

In the hypothesis generation step, the distance weighting parameter σ_d was set to 10 mm. The point-to-point geometrical correspondences $(\mathbf{p}_i, \mathbf{p}_i(d^*))$ were established in discrete steps of $p_{\text{CR}}/10$ mm; $p_{\text{CR}} = \sigma_d/\sqrt{k}$, along directions $\mathbf{u}_e(\mathbf{p}_i)$ in the range of $\pm 2 \cdot p_{\text{CR}}$ mm, requiring a total of 41 evaluations of point-to-point gradient similarities (5) for each point $\mathbf{p}_i$.

In the hypothesis selection step, the number L of random selections of three point-to-point geometrical correspondences $(\mathbf{p}_i, \mathbf{p}_i(d^*))$ has to be selected according to the rate of expected outliers, i.e., the rate of expected non-corresponding boundaries of anatomical structures that are due to different imaging modalities and corresponding artifacts in the two images undergoing registration. The parameter L was determined [32] for the 70%
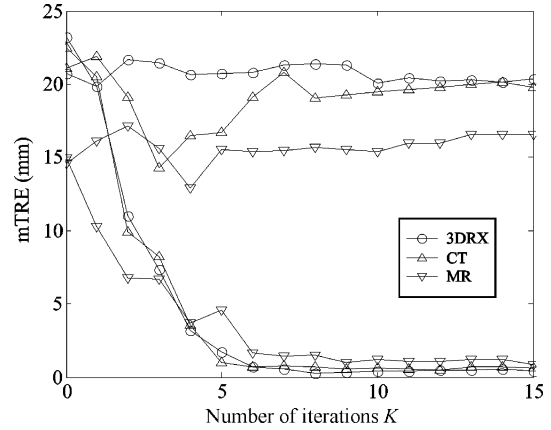
Fig. 4. Typical convergence curves of the RGRB method for the registration of 3DRX, CT and MR images to two X-ray images showing the mTRE value as a function of iterations k. For each 3-D modality, one successful registration (three bottom curves) and one unsuccessful registration (three top curves) are given.

rate of expected outliers ($w = 1 - 0.7 = 0.3$) and with 95% probability ($z = 0.95$) of randomly selecting at least one set of three ($c = 3$) outlier-free point-to-point geometrical correspondences $(\mathbf{p}_i, \mathbf{p}_i(d^*))$

$$L = \frac{\log(1 - z)}{\log(1 - w^c)} = \frac{\log(1 - 0.95)}{\log(1 - 0.3^3)} \approx 100. \quad (11)$$

The value of the number of iterations K was determined experimentally by observing typical convergence curves, i.e., by observing the mTRE as a function of iteration index k (Fig. 4). With respect to good convergence properties of the RGRB method, the value of parameter K was set to 10, although such a small number of iterations may yield suboptimal registration accuracy. To increase the registration accuracy, a considerably larger number of iterations would be required. However, a computationally more attractive solution is to use the RGRBe method that performs a coarse registration by the RGRB method with a small K, the result of which is then refined by the GRB registration method that optimizes the gradient-matching criterion function (2) by the Powell's method [40].

D. Experiments

The performances of all three variations of the gradient reconstruction-based registration method (GRB, RGRB, and RGRBe method) were assessed by the standardized evaluation methodology [33] and compared to the IB [21], GB [28], and RB [29] methods. The VOIs, containing a single vertebra, from 3DRX, CT, and MR images were registered to sets of 2, 3, 5, and 7 X-ray images, while the MR images were also registered to sets of 9 and 11 X-ray images. The same as the authors of the standardized evaluation methodology [33], we have selected the anterior-posterior (AP) and the lateral (LAT) X-ray image from the 100 acquired X-ray images for the registration of two X-ray images to 3DRX, CT and MR images. When more that two X-ray images were used for registration, the first X-ray image was always the first image acquired with the 3DRX system, while the other images were chosen so as to yield an angle between the

X-ray views of approximately 60°, 35°, 24°, 18°, and 15° for the 3, 5, 7, 9, and 11 X-ray images, respectively. For each of 3DRX, CT, and MR modalities and each set of X-ray images 1600 registrations were performed by each registration method, 200 per each of the eight VOIs, resulting in a total of more than 60.000 registrations.

Three additional experiments were performed. First, the performance of the RGRB method was assessed for more iterations in an experiment using registration of CT VOIs to two X-ray images with 30 iterations ($K = 30$).

The second additional experiment was performed to compare the proposed approach for estimating the 3-D gradients from 2-D projection images to an alternative approach by reconstructing a 3-D image from two X-ray images using the algebraic reconstruction technique (ART) followed by gradient calculation [29]. The performances of the GRB, RGRB, and RGRBe methods using the alternative gradient estimation approach were also assessed by the standardized evaluation methodology [33].

The final additional experiment was performed to assess the algorithm's robustness to outliers, i.e., to additional structures that may appear in the projection images due to medical tools in clinical settings. Since to the best of our knowledge such data sets with reference registrations are not publicly available, we simulated a tube in 3-D for each of the VOIs and projected it to the X-ray images. This was performed by a simplified model of the X-ray image generation

$$I(\mathbf{p}^{2D}) = I_0 \, e^{- \int \mu(\mathbf{p}) dp} \qquad (12)$$

where $I(\mathbf{p}^{2D})$ is the intensity of the X-ray image at point $\mathbf{p}^{2D}$, I_0 is the reference intensity, $\mathbf{p}$ is a 3-D point and μ the attenuation coefficient of the anatomy [28]. The intensities of the X-ray image with simulated medical tool $I_s(\mathbf{p}^{2D})$ were obtained as

$$I_s(\mathbf{p}^{2D}) = I_0 \, e^{- \int \mu(\mathbf{p}) dp - \int \mu_t(\mathbf{p}) dp}$$
$$= I(\mathbf{p}^{2D}) \, e^{- \int \mu_t(\mathbf{p}) dp} \qquad (13)$$

where $I_s(\mathbf{p}^{2D})$ is the simulated intensity at point $\mathbf{p}^{2D}$ and μ_t the attenuation coefficient of the simulated medical tool. Fig. 5 shows the AP and LAT X-ray images and corresponding cross-sections of the coarsely reconstructed 3-D gradient images. Registration experiments using clinically relevant CT and MR modalities and 2, 3, and 5 X-ray images were performed.

E. Results

Coarse 3-D reconstructions of 2-D gradients $\mathbf{v}^{2D}(\mathbf{p}_j^{2D})$ extracted from 2, 5, and 11 X-ray images are shown in Fig. 3 (bottom row). Reconstruction artifacts are notable in the axial cross sections (left images). In the lateral cross-sections (right images) boundaries of anatomical structures are better depicted by the reconstructed 3-D gradients even when gradients are reconstructed from only two X-ray images.

According to the standardized evaluation methodology [33], the registration results are presented in Table III by the mTREs, capture ranges, and success rates. Besides the registration results obtained for the three proposed variations of the gradient reconstruction-based method, GRB, RGRB, and RGRBe, the
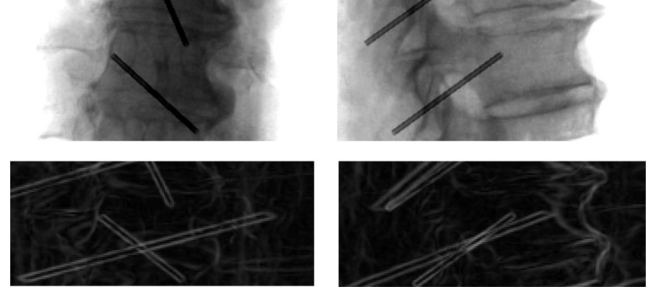
Fig. 5. Anterior–posterior (top left) and lateral (top right) X-ray images of a single vertebra with a simulated tube imitating medical tools and corresponding anterior–posterior (bottom left) and lateral (bottom right) cross sections of the coarsely reconstructed 3-D gradient images.

results of IB, GB, and RB, acquired from corresponding publications [29], [33] are also given. The RGRBe method yielded the best accuracies, capture ranges, and success rates for all three preinterventional modalities and especially when only two X-ray images were used for registration. The RGRBe method inherits the robustness of the RGRB method and the accuracy of the GRB method, which is demonstrated by scatter diagrams and convergence curves in Fig. 6.

The processing times for the GRB, RGRB ($K = 10$), and RGRBe registration methods, are presented in Table II. Processing times are independent of the number of X-ray images because the reported data do not include the times needed for coarsely reconstructing the gradient fields $\mathbf{v}(\mathbf{p})$. These times ranged from 3 to 14 s for the coarse reconstruction from 2 to 11 X-ray images, respectively. All processing times were obtained on an Intel Core 2 Duo, 2-13 GHz computer running Windows XP.

The additional experiment using 30 iterations K of the RGRB method for the CT to two X-ray registration yielded an almost identical capture range and success rate with respect to the RGRBe method with just 10 iterations (Table III, Fig. 6). However, the registration accuracy was smaller and the registration time was more than doubled, which justifies the proposed extension of the RGRB method by the optimization based GRB method, yielding better performance and higher speed.

The results of the registration methods using the gradients extracted from the reconstructed image, instead of coarsely reconstructed back-projected gradients, are presented in Table IV. By relating these results to the results in Table III, no major differences can be identified. The CT to X-ray registration with ART reconstruction was slightly more accurate but less robust, while a slight reduction of accuracy can be observed for the 3DRX and MR to X-ray registrations. The performances of the two approaches for estimating 3-D gradients from 2-D X-ray images are therefore similar but the proposed coarse 3-D gradient reconstruction is approximately 20 times faster.

The results of registration experiments using the X-ray images with the simulated medical tools are presented in Table V. In comparison to the results in Table III, a slight degradation of all registration performance criteria can be observed. For the CT to X-ray registration, the differences are very small, with the exception of the success rate of the GRB method. These results indicate that in terms of success rate the GRB method could not
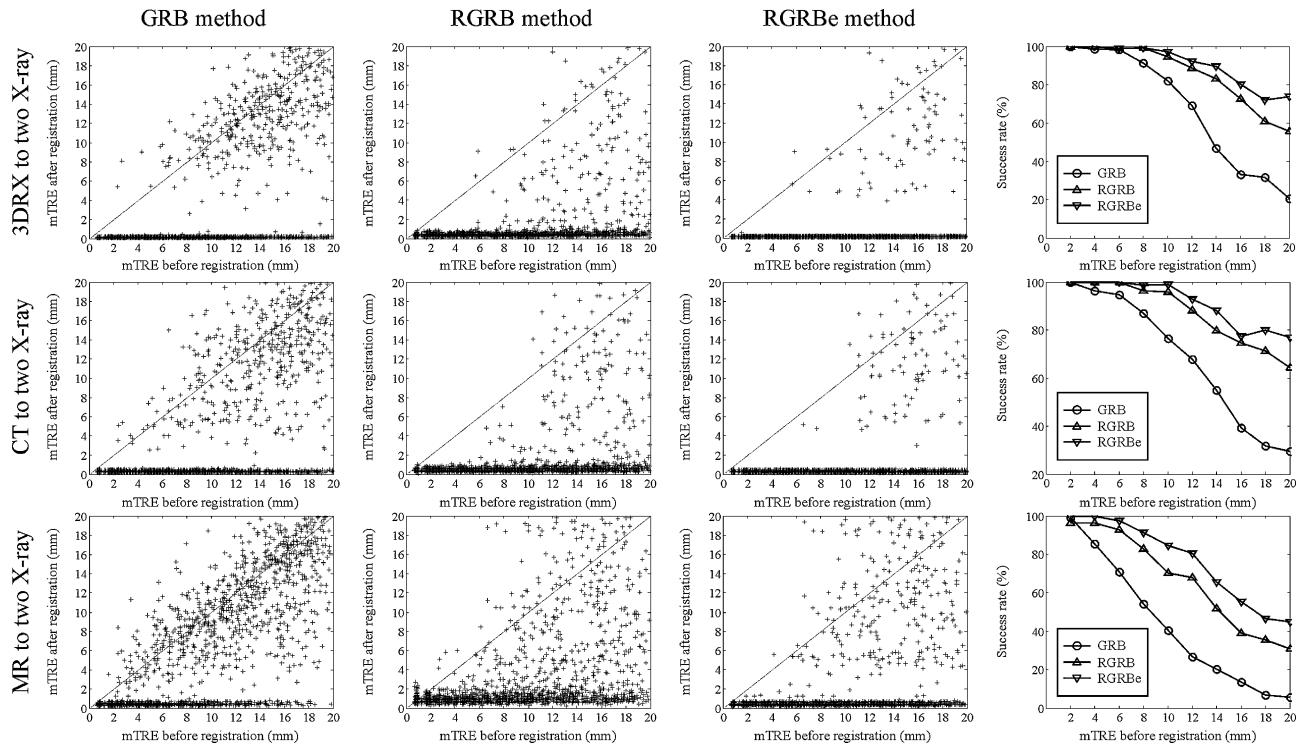
Fig. 6. Results for registration of 3DRX, CT, and MR VOIs to two X-ray images (rows, respectively) for the GRB, RGRB, and RGRBe methods (first three columns, respectively) in the form of scatter diagrams, indicating the mTRE value before and after registration. The corresponding success rates are illustrated as a function of initial mTRE (rightmost column).

TABLE II
AVERAGE PROCESSING TIMES FOR THE GRB, RGRB ($K = 10$), AND RGRBE REGISTRATION METHODS, ON AN INTEL CORE 2 DUO, 2.13-GHz COMPUTER RUNNING WINDOWS XP

Modality	Time to process (s)		
	GRB	RGRB	RGRBe
3DRX	9	18	27
CT	12	30	42
MR	15	38	53

cope well with the induced outliers in the X-ray images, while in combination with the RGRB method the success rate is not seriously impaired. MR to X-ray registration, on the other hand, was slightly more affected by the simulated outliers. While the degradation of registration performance was minor when only two X-rays were used for registration, using more X-ray images did not yield better registration results in terms of capture range and success rate. This is most likely due to the fact that when more X-ray images are used, the tools are better reconstructed and thereby represent strong outliers, which adversely affect the registration methods. This phenomenon was expectedly much less prominent for the CT images as these typically exhibit stronger bone edges.

IV. DISCUSSION

There are four important issues that need to be addressed before a 3-D/2-D registration method can be considered clinically acceptable. Namely, the registration accuracy required for a specific clinical application, the robustness of the alignment in terms of success rate and capture range, the speed with which a method can be performed, and the clinical feasibility in terms of image acquisition, user interaction, and interventional protocol requirements and/or acceptance. The proposed methods were designed with respect to these four fundamental requirements, combining the advantages of the methods proposed in the past and proposing novel solutions for overcoming their drawbacks. The performances of the proposed solutions were objectively evaluated and compared to IB [21], GB [28], and RB [29] methods via the standardized evaluation methodology [33].

Image intensity gradients proved beneficial for increasing the registration accuracy not only of the gradient-based [6], [28] but also of the intensity and reconstruction-based methods [2], [7], [8], [21]–[23], [29]. However, the local nature of intensity gradients greatly reduces the robustness of the gradient-based registration. While this is not the case for the reconstruction-based method [29], in which gradients are used as additional features, these methods typically require more intrainterventional X-ray images, which may be a serious clinical limitation both in terms of the image availability and of high computational demands required for intrainterventional reconstruction. The computational demands are also high for the intensity DRR-based methods [2], [3], [7]–[9], [20]–[23], although several solutions for acceleration were proposed [25]–[27]. Another drawback of the DRR-based methods is the projection of 3-D image data into 2-D, because of which some valuable 3-D information is inherently lost. Feature-based methods seem appealing, using point distribution or statistical anatomical models [16], [17], but the demanding model construction makes them less so. Furthermore,

TABLE III
MEAN TARGET REGISTRATION ERRORS (TRES), CAPTURE RANGES, AND SUCCESS RATES FOR DIFFERENT MODALITIES, NUMBER OF X-RAY IMAGES, AND FOR THE IB, GB, AND RB METHODS AND THE THREE VARIATIONS OF THE GRADIENT RECONSTRUCTION-BASED METHODS (GRB, RGRB, RGRBE). THE NUMBERS IN BOLD ARE THE RESULTS OF EXPERIMENTS PERFORMED IN THIS STUDY, THE NUMBERS IN PLAIN TEXT WERE TAKEN FROM [29], WHILE THE NUMBERS IN ITALIC WERE ACQUIRED FROM [33]

Modality	X-rays	mTRE (mm)						Capture range (mm)						Success rate (%)					
		IB	GB	RB	GRB	RGRB	RGRBe	IB	GB	RB	GRB	RGRB	RGRBe	IB	GB	RB	GRB	RGRB	RGRBe
3DRX	2	*0.13*	0.31	0.52	**0.19**	**0.54**	**0.17**	*4*	0	4	**6**	**9**	**11**		43	76	**69**	**86**	**91**
	3		0.19	0.33	**0.26**	**0.47**	**0.24**		7	9	**7**	**12**	**14**		68	89	**75**	**91**	**95**
	5		0.12	0.17	**0.18**	**0.37**	**0.17**		8	12	**9**	**12**	**13**		76	91	**84**	**94**	**96**
	7		0.11	0.12	**0.16**	**0.33**	**0.16**		8	12	**9**	**14**	**14**		83	92	**86**	**95**	**97**
CT	2	*0.65*	0.38	0.43	**0.32**	**0.58**	**0.32**	*3*	6	5	**5**	**9**	**11**		56	65	**69**	**88**	**92**
	3		0.32	0.37	**0.33**	**0.55**	**0.32**		7	7	**6**	**8**	**13**		63	78	**74**	**89**	**94**
	5		0.27	0.27	**0.26**	**0.43**	**0.26**		8	10	**10**	**12**	**13**		72	87	**84**	**94**	**96**
	7		0.27	0.26	**0.26**	**0.38**	**0.26**		9	12	**10**	**14**	**14**		78	91	**87**	**96**	**97**
MR	2		*0.45*		**0.50**	**1.06**	**0.48**		*1*		**2**	**4**	**6**				**44**	**68**	**69**
	3				**0.59**	**1.04**	**0.55**				**2**	**3**	**6**				**39**	**63**	**69**
	5				**0.44**	**0.94**	**0.42**				**2**	**5**	**6**				**46**	**70**	**75**
	7				**0.40**	**0.83**	**0.39**				**3**	**5**	**6**				**51**	**73**	**77**
	9		0.54	0.98	**0.42**	**0.79**	**0.37**		2	0	**2**	**8**	**9**		24	69	**54**	**74**	**78**
	11		0.50	0.67	**0.38**	**0.74**	**0.37**		2	7	**3**	**7**	**8**		23	84	**56**	**74**	**78**

TABLE IV
MEAN TARGET REGISTRATION ERRORS (TRES), CAPTURE RANGES, AND SUCCESS RATES FOR GRB, RGRB, AND RGRBE METHODS USING THE ART RECONSTRUCTION FROM TWO X-RAY IMAGES [29]

Modality	mTRE (mm)			Capture range (mm)			Success rate (%)		
	GRB	RGRB	RGRBe	GRB	RGRB	RGRBe	GRB	RGRB	RGRBe
3DRX	0.21	0.51	0.20	5	8	10	70	88	92
CT	0.28	0.53	0.27	5	9	9	68	87	90
MR	0.67	1.10	0.65	2	0	5	44	62	74

TABLE V
MEAN TARGET REGISTRATION ERRORS (TRES), CAPTURE RANGES, AND SUCCESS RATES FOR THE GRB AND RGRBE METHODS USING CT AND MR, AND 2, 3, AND 5 X-RAY IMAGES WITH SIMULATED MEDICAL TOOLS

Modality	X-rays	mTRE (mm)		Capture range (mm)		Success rate (%)	
		GRB	RGRBe	GRB	RGRBe	GRB	RGRBe
CT	2	0.34	0.34	5	10	64	88
	3	0.35	0.34	6	11	67	91
	5	0.27	0.27	8	12	63	94
MR	2	0.67	0.60	2	5	35	67
	3	0.61	0.60	2	5	37	61
	5	0.47	0.45	2	4	40	65

some feature-based methods require segmentation of pre-interventional images [4], [13]–[15], which is a very demanding task that usually requires user interaction.

To fulfill the abovementioned four clinical requirements for a 3-D/2-D registration method, a new gradient-based method has been proposed that coarsely reconstructs the 2-D gradients in 3-D. Calculated once before registration, the coarse gradient reconstruction is straightforward, computationally undemanding, and produces results comparable to those achieved by gradient extraction from reconstructed images (Table IV). The registration results (Table III) showed that the proposed optimization based GRB method outperforms the IB and GB methods in terms of success rate and capture range, which is likely due to the coarse gradient reconstruction that integrates gradient information from all the available X-ray images in 3-D. However, since medical interventions require high robustness, e.g., for the purpose of surgical guidance a success rate of 95% is typically required [6], the robust iterative RGRB registration method was proposed. In this way, the success rate and capture range were improved significantly (Table III), but because only a small number of iterations was used to keep the registration time short, the registration accuracy was not optimal. The obvious solution at hand was to extend the coarse iterative RGRB method by the fine optimization based GRB method into the coarse-to-fine RGRBe registration method. As a result, the obtained RGRBe method inherits the accuracy of the GRB method and even further increases the high robustness of the RGRB method (Fig. 6).

Finally, we compare the proposed RGRBe method with the IB, GB, and RB methods with respect to accuracy, robustness, speed, and clinical feasibility. Because it is desirable that the number of intrainterventional images is kept low, we focus on registration results when only two X-ray images were used. First, the registration accuracy of the RGRBe method was on par with the IB, GB, and RB methods, except for the 3DRX to two X-ray image registration for which the IB method was slightly more accurate. However, significant improvements in comparison with the GB and RB methods are notable when just two X-ray images were used. Furthermore, the RGRBe method was superior in MR to X-ray image registrations, yielding better accuracy with two X-ray images than the GB and RB methods with nine X-ray images.

Second, considering the robustness, i.e., the capture range and success rate, the RGRBe method has performed far the best. This was especially true for registering CT and 3DRX to two X-ray images for which the capture ranges and success rates were approximately 100% better than those of the IB, GB, and RB methods, not to mention MR to X-ray image registrations.

However, when more X-ray images had been used for registration the improvements of the capture ranges and success rates were less prominent.

Third, the registration speed is a serious drawback of the IB (9 min on a multiuser Linux Dell PowerEdge 1600, dual Xeon 2.8 GHz with 4 GB memory) and RB methods for the reasons stated above, while the GB method is rather fast (25 s on a Windows 2000 Dell Workstation PWS340 Intel Pentium 4, 1.7 GHz, 1.6 GB RAM). However, it should be noted that in the recent years the intensity-based methods were a subject of intensive research that led to much more efficient implementations. The processing times of 180 s were reported for hardware acceleration by NVidia FX 5600 graphics card with 256 MB of texture memory [8], while the processing times of 25–100 s were reported for software acceleration using a 2.2 GHz Intel Xeon processor [25]. These accelerations make the intensity-based methods feasible for clinical use. The speed of the RGRBe method depends on the number I of the extracted 3-D gradients that correspond to distinctive boundaries of anatomical structures and ranges from approximately 30–60 s on a Windows XP Intel Core 2 Duo, 2.13 GHz (Table II). The method was implemented in C++ and was not optimized for speed, although this could easily be achieved by parallelization of finding the point-to-point geometrical correspondences in the hypothesis generation step or by a more optimal determination of the number L of random selections in the hypothesis selection step, to mention but a few.

Fourth, considering the clinical feasibility, the proposed methods, as well as the IB, GB, and RB methods, do not require intrainterventional segmentation of 2-D X-ray images, which is a drawback of feature-based methods. The extraction of the set of 3-D gradients is accomplished by simple thresholding and since this is done prior to intervention, other more sophisticated methods can be used to extract less but more representative surface points of the 3-D anatomical structures of interest and thereby further improve the registration accuracy and speed. Nevertheless, the registration results demonstrate that the proposed RGRBe method outperforms the IB, GB, and RB methods in terms of registration accuracy and robustness. This is especially true when only two X-ray images are used for registration and for MR to X-ray registration, which are important advantages for numerous clinical applications. Furthermore, additional experiments (Table V) showed that for the CT to X-ray registration the proposed RGRBe method is robust to outliers like medical tools introduced in the intrainterventional X-ray images. This was not the case for the MR to X-ray registration, where outliers hampered the success rate when more than two X-rays were used for registration. Nevertheless, when only two X-rays were used, the registration accuracy and robustness were similar to the cases with no outliers also in MR to X-ray registration.

V. CONCLUSION

The advantages of gradient and reconstruction-based methods were efficiently combined into a novel robust 3-D/2-D registration method. The proposed method can register both 3-D CT and MR preinterventional images to only a few 2-D X-ray intrainterventional images. The method was thoroughly tested using the standardized evaluation methodology for 3-D/2-D registration [33] and objectively compared to some of the well-known registration methods [21], [28], [29]. The obtained results indicated better registration accuracy and robustness, especially when just a few X-ray images and when MR images were used for registration. As such, the proposed method might prove valuable in various image-guided interventions.

REFERENCES

[1] R. A. McLaughlin, J. Hipwell, D. J. Hawkes, J. A. Noble, J. V. Byrne, and T. C. Cox, "A comparison of a similarity-based and a feature-based 2-D-3-D registration method for neurointerventional use," *IEEE Trans. Med. Imag.*, vol. 24, no. 8, pp. 1058–1066, Aug. 2005.

[2] J. H. Hipwell, G. P. Penney, R. A. McLaughlin, K. Rhode, P. Summers, T. C. Cox, J. V. Byrne, J. A. Noble, and D. J. Hawkes, "Intensity-based 2-D-3-D registration of cerebral angiograms," *IEEE Trans. Med. Imag.*, vol. 22, no. 11, pp. 1417–1426, Nov. 2003.

[3] J. Weese, G. P. Penney, P. Desmedt, T. M. Buzug, D. L. G. Hill, and D. J. Hawkes, "Voxel-based 2-D/3-D registration of fluoroscopy images and CT scans for image-guided surgery," *IEEE Trans. Inf. Technol. Biomed.*, vol. 1, no. 4, p. 284, Dec. 1997.

[4] A. Gueziec, P. Kazanzides, B. Williamson, and R. H. Taylor, "Anatomy-based registration of CT-scan and intraoperative X-ray images for guiding a surgical robot," *IEEE Trans. Med. Imag.*, vol. 17, no. 5, pp. 715–28, Oct. 1998.

[5] D. Simon, R. O'Toole, M. Blackwell, F. Morgan, A. Di Gioia, and T. Kanade, "Accuracy validation in image-guided orthopaedic surgery," in *Proc. 2nd Int. Symp. Med. Robot. Comput. Assist. Surg.*, Baltimore, MD, 1995, pp. 185–192.

[6] H. Livyatan, Z. Yaniv, and L. Joskowicz, "Gradient-based 2-D/3-D rigid registration of fluoroscopic X-ray to CT," *IEEE Trans. Med. Imag.*, vol. 22, no. 11, pp. 1395–1406, Nov. 2003.

[7] M. J. Murphy, "An automatic six-degree-of-freedom image registration algorithm for image-guided frameless stereotaxic radiosurgery," *Med. Phys.*, vol. 24, no. 6, pp. 857–866, 1997.

[8] A. Khamene, P. Bloch, W. Wein, M. Svatos, and F. Sauer, "Automatic registration of portal images and volumetric CT for patient positioning in radiation therapy," *Med. Image Anal.*, vol. 10, no. 1, pp. 96–112, 2006.

[9] K. G. A. Gilhuijs, P. J. H. van de Ven, and M. van Herk, "Automatic three-dimensional inspection of patient setup in radiation therapy using portal images, simulator images, and computed tomography data," *Med. Phys.*, vol. 23, no. 3, pp. 389–399, 1996.

[10] J. R. Adler, M. J. Murphy, S. D. Chang, and S. L. Hancock, "Image-guided robotic radiosurgery," *Neurosurgery*, vol. 44, no. 6, pp. 1299–1306, 1999.

[11] J. B. Maintz and M. A. Viergever, "A survey of medical image registration," *Med. Image Anal.*, vol. 2, no. 1, pp. 1–36, 1998.

[12] C. R. Maurer, R. J. Maciunas, and J. M. Fitzpatrick, "Registration of head CT images to physical space using a weighted combination of points and surfaces," *IEEE Trans. Med. Imag.*, vol. 17, no. 5, pp. 753–761, Oct. 1998.

[13] J. Feldmar, N. Ayache, and F. Betting, "3D-2D projective registration of free-form curves and surfaces," *Comput. Vis. Image Understand.*, vol. 65, no. 3, pp. 403–424, 1997.

[14] A. Hamadeh, S. Lavallee, and P. Cinquin, "Automated 3-dimensional computed tomographic and fluoroscopic image registration," *Comput. Aided Surg.*, vol. 3, no. 1, pp. 11–19, 1998.

[15] S. Lavallee and R. Szeliski, "Recovering the position and orientation of free-form objects from image contours using 3D distance maps," *IEEE Trans. Pattern Anal. Mach. Intell.*, vol. 17, no. 4, pp. 378–390, Apr. 1995.

[16] S. Benameur, M. Mignotte, S. Parent, H. Labelle, W. Skalli, and J. de Guise, "3D/2D registration and segmentation of scoliotic vertebrae using statistical models," *Computerized Med. Imag. Graphics*, vol. 27, no. 5, pp. 321–337, 2003.

[17] G. Zheng, X. Dong, K. T. Rajamani, X. Zhang, M. Styner, R. U. Tho-ranaghatte, L.-P. Nolte, and M. A. G. Ballester, "Accurate and robust reconstruction of a surface model of the proximal femur from sparse point data and a dense point distribution model for surgical navigation," *IEEE Trans. Biomed. Eng.*, vol. 54, no. 12, pp. 2109–2122, Dec. 2007.

[18] C. R. Maurer, J. M. Fitzpatrick, M. Y. Wang, R. L. Galloway, R. J. Maciunas, and G. S. Allen, "Registration of head volume images using implantable fiducial markers," *IEEE Trans. Med. Imag.*, vol. 16, no. 4, pp. 447–462, Aug. 1997.

[19] D. Tomaževič, B. Likar, and F. Pernuš, ""Gold standard" data for evaluation and comparison of 3D/2D registration methods," *Comput. Aided Surg.*, vol. 9, no. 4, pp. 137–144, 2004.

[20] L. Lemieux, R. Jagoe, D. R. Fish, N. D. Kitchen, and D. G. T. Thomas, "A patient-to-computed-tomography image registration method based on digitally reconstructed radiographs," *Med. Phys.*, vol. 21, no. 11, pp. 1749–1760, 1994.

[21] G. P. Penney, J. Weese, J. A. Little, P. Desmedt, D. L. G. Hill, and D. J. Hawkes, "A comparison of similarity measures for use in 2-D-3-D medical image registration," *IEEE Trans. Med. Imag.*, vol. 17, no. 4, pp. 586–595, Aug. 1998.

[22] D. B. Russakoff, T. Rohlfing, A. Ho, D. H. Kim, R. Shahidi, J. R. Adler, and C. R. Maurer, "Evaluation of intensity-based 2D-3D spine image registration using clinical gold-standard data," in *2nd Int. Workshop Biomed. Image Registration*, J. C. Gee, M. J. B. A. , and V. M. W. , Eds., Philadelphia, PA, 2003, vol. 2717, pp. 151–160.

[23] G. P. Penney, P. G. Batchelor, D. L. G. Hill, D. J. Hawkes, and J. Weese, "Validation of a two- to three-dimensional registration algorithm for aligning preoperative CT images and intraoperative fluoroscopy images," *Med. Phys.*, vol. 28, no. 6, pp. 1024–1032, 2001.

[24] J. Kim, S. D. Li, D. Pradhan, R. Hammoud, Q. Chen, F. F. Yin, Y. Zhao, J. H. Kim, and B. Movsas, "Comparison of similarity measures for rigid-body CT/dual x-ray image registrations," *Technol. Cancer Res. Treatment*, vol. 6, no. 4, pp. 337–345, 2007.

[25] D. B. Russakoff, T. Rohlfing, K. Mori, D. Rueckert, A. Ho, J. R. Adler, and C. R. Maurer, "Fast generation of digitally reconstructed radiographs using attenuation fields with application to 2D-3D image registration," *IEEE Trans. Med. Imag.*, vol. 24, no. 11, pp. 1441–1454, Nov. 2005.

[26] W. Birkfellner, R. Seemann, M. Figl, J. Hummel, C. Ede, P. Homolka, X. H. Yang, P. Niederer, and H. Bergmann, "Wobbled splatting—A fast perspective volume rendering method for simulation of x-ray images from CT," *Phys. Med. Biol.*, vol. 50, no. 9, pp. N73–N84, 2005.

[27] J. Weese, R. Göcke, G. P. Penney, P. Desmedt, T. M. Buzug, and H. Schumann, "Fast voxel-based 2D/3D registration algorithm using a volume rendering method based on the shear-warp factorization," in *Medical Imaging 1999: Image Processing*, K. M. Hanson, Ed. San Diego, CA: SPIE, 1999, vol. 3661, pp. 802–810.

[28] D. Tomaževič, B. Likar, T. Slivnik, and F. Pernuš, "3-D/2-D registration of CT and MR to X-ray images," *IEEE Trans. Med. Imag.*, vol. 22, no. 11, pp. 1407–1416, Nov. 2003.

[29] D. Tomaževič, B. Likar, and F. Pernuš, "3-D/2-D registration by integrating 2-D information in 3-D," *IEEE Trans. Med. Imag.*, vol. 25, no. 1, pp. 17–27, Nov. 2006.

[30] M. Prümmer, J. Hornegger, M. Pfister, and A. Dörfler, "Multi-modal 2D-3D non-rigid registration," in *Medical Imaging 2006: Image Processing*, J. Reinhardt and J. Pluim, Eds. San Diego, CA: SPIE, 2006, vol. 6144.

[31] D. Škerl, D. Tomaževič, B. Likar, and F. Pernuš, "Evaluation of similarity measures for reconstruction-based registration in image-guided radiotherapy and surgery," *Int. J. Radiation Oncol. Biol. Phys.*, vol. 65, no. 3, pp. 943–953, 2006.

[32] M. A. Fischler and R. C. Bolles, "Random sample consensus—A paradigm for model-fitting with applications to image-analysis and automated cartography," *Commun. ACM*, vol. 24, no. 6, pp. 381–395, 1981.

[33] E. B. van de Kraats, G. P. Penney, D. Tomaževič, T. van Walsum, and W. J. Niessen, "Standardized evaluation methodology for 2-D-3-D registration," *IEEE Trans. Med. Imag.*, vol. 24, no. 9, pp. 1177–1189, Sep. 2005.

[34] E. B. van de Kraats, T. van Walsum, L. Kendrick, N. J. Noordhoek, and W. J. Niessen, "Accuracy evaluation of direct navigation with an isocentric 3D rotational X-ray system," *Med. Image Anal.*, vol. 10, no. 2, p. 113, 2006.

[35] P. Markelj, D. Tomaževič, F. Pernus, and B. Likar, "Optimizing bone extraction in MR images for 3D/2D gradient based registration of MR and X-ray images," in *Medical Imaging 2007: Image Processing*, J. Reinhardt and J. Pluim, Eds. San Diego, CA: SPIE, 2007, vol. 6512.

[36] P. Jannin, C. Grova, and C. Maurer, "Model for defining and reporting reference-based validation protocols in medical image processing," *Int. J. Comput. Assist. Radiol. Surg.*, vol. 1, no. 2, p. 63, 2006.

[37] F. Maes, A. Collignon, D. Vandermeulen, G. Marchal, and P. Suetens, "Multimodality image registration by maximization of mutual information," *IEEE Trans. Med. Imag.*, vol. 16, no. 2, pp. 187–198, Apr. 1997.

[38] E. B. van de Kraats, T. van Walsum, J. J. Verlaan, F. C. Oner, M. A. Viergever, and W. J. Niessen, "Noninvasive magnetic resonance to three-dimensional rotational X-ray registration of vertebral bodies for image-guided spine surgery," *Spine*, vol. 29, no. 3, pp. 293–297, 2004.

[39] B. Likar, M. A. Viergever, and F. Pernuš, "Retrospective correction of MR intensity inhomogeneity by information minimization," *IEEE Trans. Med. Imag.*, vol. 20, no. 12, pp. 1398–1410, Dec. 2001.

[40] W. H. Press, S. A. Teukolsky, W. T. Vetterling, and B. P. Flannery, *Numerical Recipes in C++*, 2nd ed. Cambridge, U.K.: Cambridge Univ. Press, 1992.